Beyond modelocking: High repetition-rate frequency combs derived from a continuous-wave laser

by

Daniel C. Cole

B.S., Washington University in St. Louis, 2012

M.S., University of Colorado, 2015

A thesis submitted to the

Faculty of the Graduate School of the

University of Colorado in partial fulfillment

of the requirements for the degree of

Doctor of Philosophy

Department of Physics

2018

This thesis entitled:
Beyond modelocking: High repetition-rate frequency combs derived from a continuous-wave laser
written by Daniel C. Cole
has been approved for the Department of Physics

_____

Reader1

_____

Reader2

Date _____

The final copy of this thesis has been examined by the signatories, and we find that both the content and the form meet acceptable presentation standards of scholarly work in the above mentioned discipline.

Cole, Daniel C. (Ph.D., Physics)

Beyond modelocking: High repetition-rate frequency combs derived from a continuous-wave laser

Thesis directed by Dr. Scott A. Diddams

Optical frequency combs based on modelocked lasers have revolutionized precision metrology by enabling measurements of optical frequencies, with implications both for fundamental scientific questions and for applications such as fast, broadband spectroscopy. In this thesis, I describe advances in the generation of frequency combs without modelocking in platforms with smaller footprints and higher repetition rates, with the ultimate goal of bringing frequency combs to new applications in a chip-integrated package. I discuss two approaches for comb generation: parametric frequency conversion in Kerr microresonators and active electro-optic modulation of a continuous-wave laser. After introducing microresonator-based frequency combs (microcombs), I discuss two specific developments in microcomb technology: First, I describe a new, extremely reliable method for generation of soliton pulses through the use of a phase-modulated pump laser. This technique removes the dependence on initial conditions that was formerly a universal feature of these experiments, presenting a solution to a significant technical barrier to the practical application of microcombs. Second, I present observations of 'soliton crystal' states with highly structured 'fingerprint' optical spectra that correspond to ordered pulse trains exhibiting crystallographic defects. These pulse trains arise through interaction of solitons with avoided mode-crossings in the resonator spectrum. I also discuss generation of Kerr soliton combs in the Fabry-Perot (FP) geometry, with a focus on the differences between the FP geometry and the ring geometry that has been the choice of most experimenters to date. Next, I present results on combs based on electro-optic modulation. I discuss the operational principle, and then describe the first self-referencing of a frequency comb of this kind and a proof-of-principle metrology experiment. Finally, I discuss a technique for reducing the repetition rate of a high-repetition-rate frequency comb, which will be a necessary post-processing step for some applications. I conclude with a discussion of avenues for future research.

Contents

Figures

Chapter 1

Introduction

The invention of the optical frequency comb two decades ago initiated a revolution in precision measurement by dramatically improving the resolution with which we can conveniently measure time and frequency [1–5]. This revolution was brought about by the realization of a simple scheme[1] by which the hundreds-of-terahertz-scale optical frequencies of a modelocked laser could be measured electronically, and was facilitated by the development of high performing solid-state femtosecond laser technology such as the Ti:sapphire laser. Optical frequency combs have found important roles in experiments and applications in contexts including the first demonstration of an optical atomic clock [7], systems for ultra-low-noise microwave synthesis [8], broadband spectroscopy applications [9, 10], optical arbitrary waveform generation [11], and stable long-term calibration of astronomical spectrographs for exoplanet detection [12]. Further development of the technology beyond the first stabilization of the Ti:sapphire laser that heralded the frequency comb's arrival has enabled combs to reach applications across many wavelength bands [13–16]. The technology is reaching maturity, and frequency combs have been commercially available for some time.

In the last decade, methods for generating optical frequency combs without a modelocked laser have begun to suggest new ways to bring their capabilities to applications outside the controlled environment of the research laboratory. These new frequency combs come with higher repetition rates, and this makes them particularly attractive for applications where high power per comb mode, individual accessibility of comb modes, and fast acquisition times are desired. These applications

[1] that required markedly *less* simple advancements in capabilities in nonlinear optics [6].

include arbitrary microwave and optical waveform generation, telecommunications, and broadband, fast-acquisition-time spectroscopy. Moreover, these combs come with lower size, weight, and power (SWAP) requirements, which will enable them to bring the features that make modelocked-laser-based combs attractive into the field, enabling e.g. direct optical frequency synthesis on a chip [17].

This thesis focuses on these new approaches for frequency comb generation. The bulk of the thesis covers microresonator-based frequency combs, and especially the nonlinear dynamics involved in the generation of these frequency combs via the Kerr nonlinearity; an introduction to this field is provided in Chapter **??**. Chapters **??**-**??** describe advancements in the field. Chapter **??** presents a second method for generating a high-repetition-rate frequency comb without modelocking that is based on active modulation of a CW seed laser and subsequent nonlinear spectral broadening. In Chapter **??**, I present experimental and theoretical investigations of repetition-rate reduction of frequency combs via pulse gating, which may prove useful for adapting low-SWAP combs and their intrinsically high repetition rates to some applications as the technology continues to develop. Finally, in Chapter **??** I discuss avenues for further research.

In the remainder of this chapter, I discuss the basic properties of frequency combs and explain how the optical frequencies making up a comb can be fully determined by electronics operating with gigahertz-scale bandwidths.

1.1 Optical frequency combs

An optical frequency comb is obtained by fully stabilizing the spectrum of an optical pulse train. The first frequency combs came about through full frequency-stabilization of modelocked lasers; this thesis focuses on frequency combs with pulse trains generated through other means.

1.1.1 Optical pulse trains and their spectra

In the time domain, a frequency comb consists of a train of uniformly spaced optical pulses arriving at the pulse train's repetition rate f_{rep}, which within the rapidly expanding space of frequency

comb technology is between ∼10 MHz and ∼1 THz. These pulses are typically very short compared to their repetition period $T = 1/f_{rep}$, with durations on the order of 100 fs. In the frequency domain, the comb consists of a set of modes that are spaced by f_{rep} in frequency and that have amplitudes determined by an overall spectral envelope centered at the optical carrier frequency ν_c (∼193 THz in this thesis), with bandwidth inversely related to the temporal duration of the pulses. The usual description of a frequency comb, which is natural for modelocked-laser-based combs that are not derived from a CW laser, gives the frequencies of these modes as

$$\nu_n = nf_{rep} + f_0, \tag{1.1}$$

where $n \sim \nu_c/f_{rep}$ for the optical modes that make up the comb and f_0 is the carrier-envelope offset frequency, which may be defined to be between 0 and f_{rep}. The offset frequency results from the pulse-to-pulse evolution of the carrier wave underneath the temporal intensity envelope of the pulses due to a difference in group and phase velocities. An equivalent representation of the frequencies of the comb that is more natural for frequency combs directly derived from a CW laser, as described in this thesis, is

$$\nu_\mu = \nu_c + \mu f_{rep}, \tag{1.2}$$

where ν_c is the frequency of the CW laser, the 'pump' or 'seed' laser, from which the frequency comb is derived and μ is a pump-referenced mode number, in contrast with the zero-referenced mode number n of Eq. 1.1. Now the carrier-envelope offset frequency f_0 is found in the difference between ν_c and the closest harmonic of f_{rep}: $f_0 = \nu_c - Nf_{rep}$, where N is the largest integer such that $f_0 > 0$. Fig. 1.1 depicts the properties of a frequency comb in the time domain and the frequency domain.

It is useful to consider a mathematical treatment of an optical pulse train to understand the relationships presented above. In the time domain, the electric field $E(t)$ of the pulse train consists of optical pulses that arrive periodically and have baseband (centered at zero frequency) field envelope $A(t)$ multiplying the carrier wave of angular frequency $\omega_c = 2\pi\nu_c$:

$$E(t) = \sum_{k=-\infty}^{\infty} A(t - kT)e^{i\omega_c t}. \tag{1.3}$$

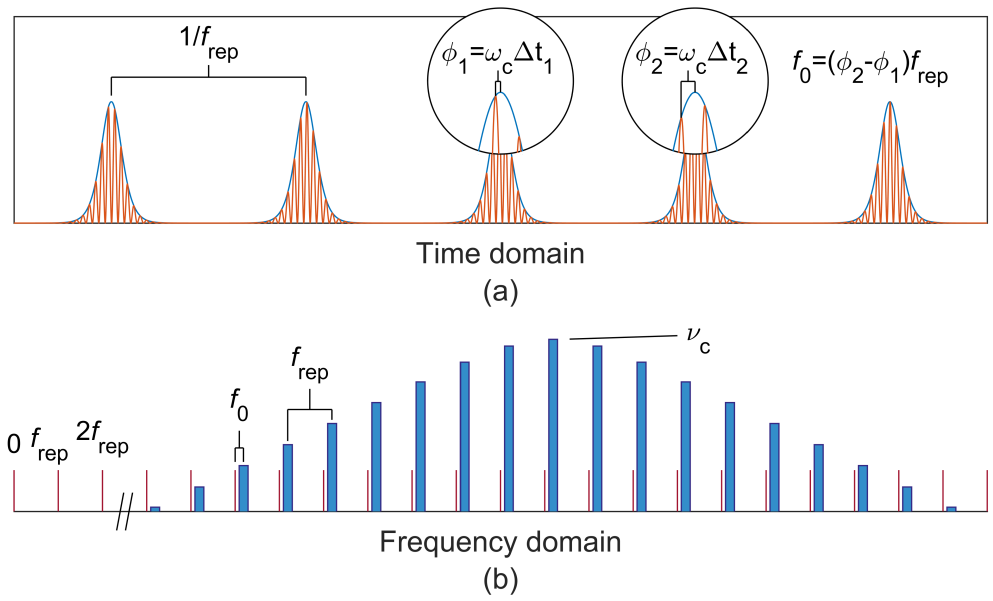

Figure 1.1: **Optical frequency combs in the time and frequency domains.** (a) Time-domain depiction of a frequency comb as a train of pulses spaced by $1/f_{rep}$. The intensity envelope is shown in blue, and the carrier wave is shown in orange. The carrier-envelope offset frequency f_0 arises from a phase-slip of the carrier with respect to the intensity envelope from pulse to pulse. Specifically, if phases $\phi_j = \omega_c \Delta t_j$ are traced out by the carrier wave between its maximum and the j^{th} peak of the pulse train, then $f_0 = \frac{\phi_{j+1}-\phi_j}{2\pi} f_{rep}$. (b) Frequency-domain depiction of the same frequency comb. The comb modes (shown in blue) are centered around an optical frequency ν_c and offset from harmonics of the repetition rate f_{rep} (shown in red) by a frequency shift f_0. Note that the x-axis has been broken, and the zero-referenced mode numbers of the comb modes shown are large, e.g. $n \sim 19340$ for a 10 GHz repetition-rate comb centered at 1550 nm wavelength (see Chapter **??**).

Here, T is the repetition period of the pulse train. Eq. 1.3 can be viewed as describing a laser of angular frequency ω_c with a time-varying amplitude. This temporal modulation leads to the distribution of the power across a spectrum whose width scales inversely with the temporal duration of A. Intuitively, the spectrum of the comb is the spectrum of the periodic baseband field envelope[2] $\Sigma_k A(t-kT)$, shifted by the multiplication with $e^{i\omega_c t}$ so that it is centered around the optical carrier. More formally, we can calculate the frequency content of the comb by calculating

$$\mathcal{F}\{E\}(\omega) \sim \left(\sum_{k=-\infty}^{\infty} \mathcal{F}\{A(t-kT)\} \right) * \delta(\omega - \omega_c), \tag{1.4}$$

which results from the convolution (denoted by $*$) theorem for Fourier transforms; $\mathcal{F}$ denotes Fourier transformation. We use the Fourier transform's property that a temporal translation results in a

[2] which, as the spectrum of a periodic function, is already a comb.

linear spectral phase shift to obtain:

$$\mathcal{F}\{E\} \sim \left(\mathcal{F}\{A\} \times \sum_{k=-\infty}^{\infty} e^{-i\omega kT} \right) * \delta(\omega - \omega_c). \tag{1.5}$$

The quantity $\Sigma_k e^{-i\omega kT}$ is the Fourier-series representation of the series of δ-functions $\Sigma_\mu \delta(\omega - 2\pi\mu/T)$, so we have

$$\mathcal{F}\{E\}(\omega) \sim \left(\mathcal{F}\{A\} \times \sum_{\mu=-\infty}^{\infty} \delta(\omega - 2\pi\mu/T) \right) * \delta(\omega - \omega_c), \tag{1.6}$$

and performing the convolution leads to the replacement of ω with $\omega - \omega_c$, leading to:

$$\mathcal{F}\{E\} \sim \sum_{\mu=-\infty}^{\infty} \delta(\omega - \omega_c - \mu\omega_r)\, \mathcal{F}\{A\}(\omega - \omega_c), \tag{1.7}$$

where $\omega_{rep} = 2\pi f_{rep} = 2\pi/T$. This expression indicates that the spectrum of the comb has frequency content at modes $\nu_\mu = \nu_c + \mu f_{rep}$, and that their amplitudes are determined by the spectrum of the baseband field envelope, shifted up to the optical carrier frequency ν_c. This is the natural formulation in the case of a comb derived from a CW laser, but it obscures the carrier-envelope offset frequency in the difference between ν_c and the nearest multiple of the repetition rate, as discussed above. In practice, if f_{rep} is known, then a measurement of f_0 is equivalent to a measurement of the frequency of the input CW laser.

1.1.2 Frequency stabilization of optical pulse trains

The scientific need for a method to measure optical frequencies motivated the development of optical frequency combs. While the measurement bandwidth of electronic frequency counters has improved since 1999, it remains limited to frequencies roughly one *million* times lower than the frequency of, e.g., visible red light. Frequency combs present a method for measurement of the unknown frequency f_{opt} of an optical signal through heterodyne with a frequency comb—if f_{opt} falls within the bandwidth of the frequency comb, then the frequency of the heterodyne between the comb and the signal is guaranteed to be less than $f_{rep}/2$, which at least for modelocked-laser-based combs can be measured electronically. Therefore, if the frequencies of the comb are known, measurement of the heterodyne of the comb with the signal reveals the frequency of the signal, provided that the

comb mode number and sign of the beat can be determined. This can be done via a wavelength measurement if sufficient precision is available, or by measuring the change $\partial f_b/\partial f_{rep}$, where f_b is the measured frequency of the beat.

The unique utility of the optical frequency comb lies in the fact that measurement of the two microwave frequencies f_{rep} and f_0, along with a measurement of the spectral envelope, is sufficient to determine the optical frequencies of all of the modes of the comb, thereby enabling frequency measurement of optical signals. Measurement of the repetition rates of optical pulse trains was possible for many years before the realization of optical frequency comb technology, as this can be done by simply impinging the pulse train on a photodetector. It was the confluence of several technological developments around the turn of the twenty-first century that allowed detection and measurement of the carrier-envelope offset frequency, thereby enabling creation of fully-stabilized modelocked-laser pulse trains: optical frequency combs.

The carrier-envelope offset frequency of a pulse train is challenging to measure because it describes evolution of the optical carrier wave underneath the intensity envelope, and therefore cannot be measured through straightforward detection of the intensity of the pulse train. Presently, the most straightforward way to measure f_0 is $f-2f$ *self-referencing*. This can be performed only with a pulse train whose spectrum spans an octave—a factor of two in frequency. Given such an octave-spanning supercontinuum spectrum, a group of modes near mode number N is frequency-doubled in a medium with the $\chi^{(2)}$ nonlinearity [18]. This frequency-doubled light is heterodyned with the native light in the supercontinuum with mode number near $2N$. The frequency of the resulting beat f_b is:

$$f_b = f_{doubled} - f_{native} \tag{1.8}$$

$$= 2(Nf_{rep} + f_0) - (2Nf_{rep} + f_0) \tag{1.9}$$

$$= f_0. \tag{1.10}$$

Such a scheme is typically performed in a '$f-2f$ interferometer,' which is depicted in Fig. 1.2. Generating the necessary octave-spanning supercontinuum spectrum typically requires nonlinear

spectral broadening of the pulse train after its initial generation, except for in specific, carefully engineered cases (e.g. [19]). Achieving the required degree of spectral broadening while preserving the coherence properties of the pulse train is a significant challenge—in the past this has typically required launching a train of high energy ($\sim$1 nJ), temporally short ($\leq$ 100 fs) pulses into the spectral-broadening stage. Recent developments in nonlinear waveguide technology have relaxed these requirements slightly (e.g. Ref. [20]), but maintaining the coherence of the pulse train during spectral broadening remains one of the important engineering considerations in designing optical frequency comb systems, as discussed in Chapters **??** and **??**.

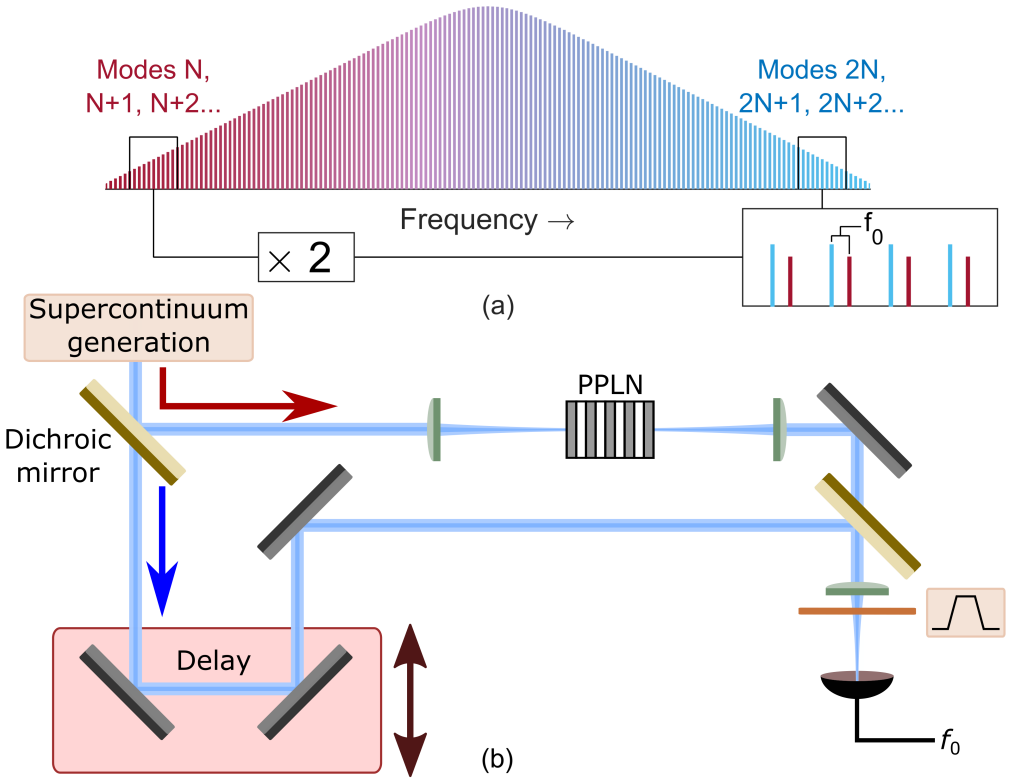

Figure 1.2: **Measurement of the carrier-envelope offset frequency f_0 via $f-2f$ self-referencing.** (a) Frequency-domain depiction of $f-2f$ self-referencing: Light on the low frequency end of an octave-spanning supercontinuum is frequency-doubled, and then heterodyned with light on the high frequency end near twice its frequency, enabling measurement of the carrier-envelope offset frequency. (b) Schematic depiction of a basic $f-2f$ interferometer: After supercontinuum generation, a dichroic mirror splits the light by wavelength, and the low-frequency end of the supercontinuum is sent (red arrow) through a nonlinear crystal for frequency-doubling. Here the crystal is periodically-poled lithium niobate (PPLN), where quasi-phase-matching is employed for efficient doubling of the target modes. The high-frequency end is sent (blue arrow) through a delay stage, which can be adjusted to compensate for temporal walk-off between spectral the components (modes $\sim N$ and modes $\sim 2N$) required for self-referencing during the supercontinuum-generation process. The paths are then re-combined by a second dichroic mirror and sent through a narrow optical band-pass filter centered around the doubled modes, which filters out unneceessary light and increases the signal-to-noise ratio of the detected f_0 signal. Photdetection of the band-passed beam then reveals f_0.

Appendix A

Numerical simulations of nonlinear optics

This appendix describes the algorithm used for numerical simulation of the generalized nonlinear Schrodinger equation (GNLSE) and Lugiato-Lefever equation (LLE) to obtain the results presented in the preceding chapters in this thesis. These equations are simulated with Matlab using a fourth-order Runge-Kutta interaction picture (RK4IP) method [144] with adaptive step size [143]. The RK4IP method is a particular algorithm in the broader class of split-step Fourier algorithms, in which nonlinearity is implemented in the time domain and dispersion is implemented in the frequency domain. An illustrative example of this split-step Fourier approach is a far simpler algorithm carried out with a single line of Matlab code to simulate the LLE:

```
psi=ifft(exp(delta*L).*fft(exp(delta*(1i*abs(psi).^2+F./psi)).*psi));
```

where `delta` is the step size and `L` is a linear frequency-domain dispersion operator ($\hat{L}$, see below) that has been defined in the preceding code. The RK4IP algorithm with adaptive step size is advantageous over this simple algorithm in calculation time and in the scaling of error with the step size.

A.1 RK4IP algorithm

The LLE (NLSE) describes the evolution of the field ψ (A), a function of a fast variable θ (T), over a timescale parametrized by a slow variable τ (z). In what immediately follows we use the variable names corresponding to the LLE for simplicity. Each of these equations can be written as the sum of a nonlinear operator $\hat{N}$ and a linear operator $\hat{L}$ acting on ψ, so that the field ψ evolves

as

$$\frac{\partial \psi}{\partial \tau} = (\hat{N} + \hat{L})\psi, \tag{A.1}$$

which can be implemented with the split-step Fourier approach.

The RK4IP algorithm specifies a recipe for advancing the field a single step δ in the slow variable τ to obtain $\psi(\theta, \tau + \delta)$ from $\psi(\theta, \tau)$. This specific algorithm has the attractive feature that it reduces the number of Fourier transformations that must be performed to achieve a given calculation accuracy relative to other common algorithms. The RK4IP algorithm is[144]:

$$\psi_I = \exp\left(\frac{\delta}{2}\hat{L}\right)\psi(\theta,\tau) \tag{A.2}$$

$$k_1 = \exp\left(\frac{\delta}{2}\hat{L}\right)\left[\delta\tau\hat{N}(\psi(\theta,\tau))\right]\psi(\theta,\tau) \tag{A.3}$$

$$k_2 = \delta\hat{N}(\psi_I + k_1/2)\left[\psi_I + k_1/2\right] \tag{A.4}$$

$$k_3 = \delta\hat{N}(\psi_I + k_2/2)\left[\psi_I + k_2/2\right] \tag{A.5}$$

$$k_4 = \delta\hat{N}\left(\exp\left(\frac{\delta}{2}\hat{L}\right)(\psi_I + k_3)\right) \tag{A.6}$$

$$\times \exp\left(\frac{\delta}{2}\hat{L}\right)(\psi_I + k_3) \tag{A.7}$$

$$\psi(\theta,\tau+\delta) = \exp\left(\frac{\delta}{2}\hat{L}\right)\left[\psi_I + k_1/6 + k_2/3 + k_3/3\right] + k_4/6. \tag{A.8}$$

In the above it is understood that $\hat{L}$ is applied in the frequency domain and $\hat{N}$ is applied in the time domain. Calculation of $\psi(\theta, \tau+\delta)$ from $\psi(\theta, \tau)$ therefore requires eight Fourier transformations.

A.2 Adaptive step-size algorithm

An adaptive step-size algorithm is a strategy for adjusting the magnitude of the steps δ that are taken to optimize the simulation speed while maintaining a desired degree of accuracy. The RK4IP algorithm exhibits error that scales locally as $O(\delta^5)$. Since reducing the step size naturally requires more steps and therefore increases the number of small errors that accumulate, the resulting global accuracy of the algorithm is $O(\delta^4)$. One appropriate step-size adjustment algorithm for this scaling is described by Heidt [143]. For a given goal error e_G, the algorithm goes as follows:

- Calculate a field ψ_{coarse} by advancing the field $\psi(\theta, \tau)$ according to RK4IP by a step of size δ.

- Calculate a field ψ_{fine} by advancing the field $\psi(\theta, \tau)$ according to RK4IP by two steps of size $\delta/2$.

- Calculate the measured error $e = \sqrt{\sum_j |\psi_{coarse,j} - \psi_{fine,j}|^2 / \sum_j |\psi_{fine,j}|^2}$, where j indexes over the discrete points parametrizing the fast variable θ.

  * If $e > 2e_G$, discard the solution and repeat the process with coarse step size $\delta' = \delta/2$.

  * If $e_G < e < 2e_G$, the evolution continues and the step size is reduced to $\delta' = \delta/2^{1/5} \approx 0.87\delta$.

  * If $e_G/2 < e < e_G$, the evolution continues and the step size is not changed.

  * If $e < e_G/2$, the evolution continues and the step size is increased to $\delta' = 2^{1/5}\delta \approx 1.15\delta$.

When the simulation continues, the new field $\psi(\theta, \tau+\delta)$ is taken to be $\psi(\theta, \tau+\delta) = 16\psi_{fine}/15 - \psi_{coarse}/15$. In the calculations described in this thesis, the goal error e_G is typically 10^{-6}.

A.3 Pseudocode for numerical simulation with the RK4IP algorithm and adaptive step size

The pseudocode shown in Algorithm 1 shows how the RK4IP algorithm with adaptive step size is implemented. This pseudocode neglects the specific details of the RK4IP algorithm.

Two notes:

- The current field $\psi(\theta, \tau)$ is stored until the approximation to the new field $\psi(\theta, \tau + \delta)$ is found to be acceptable.

- This implementation makes use of an extra efficiency that is possible when the solution is discarded and the step size is halved: the first step of the fine solution $\psi_{fine,1}$ for the previous attempt becomes the coarse solution ψ_{coarse} for the current attempt.

Algorithm 1 Pseudocode showing the implementation of RK4IP with adaptive step size.

procedure
  while $\tau < \tau_{end}$ **do**
    $e = 1$ ▷ Initialize the error to a large value
    $firsttry = TRUE$ ▷ For more efficiency if this is not the first attempt (see below)
    $\delta = 2\delta$ ▷ To account for halving on the first iteration

    while $e > 2e_G$ **do**
      if $firsttry$ **then**
        $\psi_{coarse} = \mathrm{RK4IP}(\psi, \delta)$
      else
        $\psi_{coarse} = \psi_{fine,1}$ ▷ We get to re-use the first step of the previous attempt's fine solution

      $\delta = \delta/2$
      $\psi_{fine} = \psi$

      for $j_{step} = 1 : 2$ **do**
        $\psi_{fine} = \mathrm{RK4IP}(\psi_{fine}, \delta)$
        if $j_{step} = 1$ **then**
          $\psi_{fine,1} = \psi_{fine}$

      $e = \sqrt{\sum |\psi_{coarse} - \psi_{fine}|^2 / \sum |\psi_{fine}|^2}$
      $firsttry = FALSE$

    $\psi = 16\psi_{fine}/15 - \psi_{coarse}/15$
    $\tau = \tau + 2\delta$ ▷ We took two fine steps of size δ

    if $e > e_G$ **then**
      $\delta = \delta/2^{1/5}$
    if $e < e_G/2$ **then**
      $\delta = 2^{1/5}\delta$

A.3.1 Simulation of the LLE

For simulation of the LLE, the operators are:

$$\hat{N} = i|\psi|^2 + F/\psi, \tag{A.9}$$

$$\hat{L} = -(1 + i\alpha_\mu), \text{where} \tag{A.10}$$

$$\alpha_\mu = \alpha - \sum_{n=1}^{N} \beta_n \mu^n / n!. \tag{A.11}$$

The subscript μ indicates the pump-referenced mode number upon which the operator acts. Note, in particular, that the pump term F has been incorporated into the nonlinear operator, so that it is implemented in the time domain. The quantity $\hat{N}\psi$ then becomes $i|\psi|^2\psi + F$, as required for computation of $\partial\psi/\partial\tau$.

A.3.2 Simulation of the GNLSE

In addition to self-phase modulation, the GNLSE used in the simulations conducted for Chapter **??** contains nonlinear terms that describe the medium's Raman response and self-steepening. The equation employed can be written as [37, 144]:

$$\frac{\partial A}{\partial z} = -\left(\sum_n \beta_n \frac{i^{n-1}}{n!}\frac{\partial^n}{\partial T^n}\right) A + i\gamma\left(1+\frac{1}{\omega_0}\frac{\partial}{\partial T}\right) \times \left((1-f_R)A|A|^2 + f_R A\int_0^\infty h_R(\tau)|A(z,T-\tau)|^2 d\tau\right). \quad \text{(A.12)}$$

For Chapter **??**, second- and third-order dispersion is used with β_2 =-7.7 ps^2/km and β_3 =0.055 ps^3/km, where β_n is the n^{th} frequency-derivative of the propagation constant. The nonlinear coefficient $\gamma = \frac{2\pi}{\lambda}\frac{n_2}{A_{eff}}$ used is 11 W/km [138], coming from an effective mode-field diameter of ∼3.5 μm for the HNLF used in the experiment and the nonlinear index $n_2 = 2.7\times10^{-16}$ cm^2/W of silica. The quantity $\omega_0 = 2\pi c/\lambda_0$ is the (angular) carrier frequency of the pulse, and the parameter $f_R = 0.18$ and function

$$h_R(\tau > 0) = (\tau_1^2+\tau_2^2)/(\tau_1\tau_2^2)\times e^{-\tau/\tau_2}\sin\tau/\tau_1 \quad \text{(A.13)}$$

describe the medium's Raman response, with $\tau_1 = 12.2$ fs and $\tau_2 = 32$ fs used here [37, 144, 147].

The linear frequency-domain operator applied in the RK4IP algorithm is

$$\hat{L} = i\frac{\beta_2}{2}(\omega_\mu-\omega_0)^2 - \frac{\beta_3}{6}(\omega_\mu-\omega_0)^3 \quad \text{(A.14)}$$

Here ω_μ is defined by the discretization of the frequency domain due to Fourier-transformation of a finite temporal window of length T_{comp} via $\omega_\mu = \omega_0 + 2\pi\mu/T_{comp}$; where T_{comp} is the size of the domain for the fast time variable T.

The nonlinear operator $\hat{N}$ for the GNLSE implements the convolution as a product in the frequency domain. That is,

$$\hat{N} = i\gamma\frac{1}{A}\left(1+\frac{1}{\omega_0}\frac{\partial}{\partial T}\right)\times\left[(1-f_R)A|A|^2 + f_R A\,\mathcal{F}^{-1}\left\{\chi_R\cdot\mathcal{F}(|A|^2)\right\}\right], \quad \text{(A.15)}$$

where $\chi_R = \mathcal{F}\{h_R(\tau)\}$ and $\mathcal{F}$ denotes Fourier transformation. Procedurally, the quantity in the square brackets is calculated first, and then the fast-time derivative is implemented and the sum in the curved brackets is calculated.

References

[1] S. A. Diddams, D. J. Jones, J. Ye, S. T. Cundiff, J. L. Hall, J. K. Ranka, R. S. Windeler, R. Holzwarth, T. Udem, and T. W. Hänsch. Direct link between microwave and optical frequencies with a 300 THz femtosecond laser comb. *Physical Review Letters*, 84 (22), **2000**, 5102–5105. DOI: 10.1103/PhysRevLett.84.5102 (cited on page 1).

[2] D. J. Jones, S. A. Diddams, J. K. Ranka, A. Stentz, R. S. Windeler, J. L. Hall, and S. T. Cundiff. Carrier-Envelope Phase Control of Femtosecond Mode-Locked Lasers and Direct Optical Frequency Synthesis. *Science*, 288 (5466), **2000**, 635–639 (cited on page 1).

[3] T. Udem, R Holzwarth, and T. W. Hänsch. Optical frequency metrology. *Nature*, 416 (6877), **2002**, 233–237. DOI: 10.1038/416233a (cited on page 1).

[4] J. L. Hall. Nobel lecture: Defining and measuring optical frequencies. *Reviews of Modern Physics*, 78 (4), **2006**, 1279–1295. DOI: 10.1103/RevModPhys.78.1279 (cited on page 1).

[5] T. W. Hänsch. Nobel lecture: Passion for precision. *Reviews of Modern Physics*, 78 (4), **2006**, 1297–1309. DOI: 10.1103/RevModPhys.78.1297 (cited on page 1).

[6] J. K. Ranka, R. S. Windeler, and A. J. Stentz. Visible continuum generation in air–silica microstructure optical fibers with anomalous dispersion at 800 nm. *Optics Letters*, 25 (1), **2000**, 25. DOI: 10.1364/OL.25.000025 (cited on page 1).

[7] S. A. Diddams, T. Udem, J. C. Bergquist, E. A. Curtis, R. E. Drullinger, L Hollberg, W. M. Itano, W. D. Lee, C. W. Oates, K. R. Vogel, and D. J. Wineland. An Optical Clock Based on a Single Trapped 199 Hg+ Ion. *Science (New York, N.Y.)*, 293, **2001**, 825–828. DOI: 10.1126/science.1061171 (cited on page 1).

[8] T. M. Fortier, M. S. Kirchner, F. Quinlan, J. Taylor, J. C. Bergquist, T. Rosenband, N. Lemke, A. Ludlow, Y. Jiang, C. W. Oates, and S. A. Diddams. Generation of ultrastable microwaves via optical frequency division. *Nature Photonics*, 5 (7), **2011**, 425–429. DOI: 10.1038/nphoton.2011.121. arXiv: 1101.3616 (cited on page 1).

[9] S. A. Diddams, L. Hollberg, and V. Mbele. Molecular fingerprinting with the resolved modes of a femtosecond laser frequency comb. *Nature*, 445 (7128), **2007**, 627–630. DOI: 10.1038/nature05524 (cited on page 1).

[10] I. Coddington, N. Newbury, and W. Swann. Dual-comb spectroscopy. *Optica*, 3 (4), **2016**, 414–426. DOI: 10.1364/OPTICA.3.000414 (cited on page 1).

[11] S. T. Cundiff and A. M. Weiner. Optical arbitrary waveform generation. *Nature Photonics*, 4 (11), **2010**, 760–766. DOI: 10.1038/nphoton.2010.196 (cited on page 1).

[12] T. Steinmetz, T. Wilken, C. Araujo-Hauck, R. Holzwarth, T. W. Hänsch, L. Pasquini, A. Manescau, S. D'Odorico, M. T. Murphy, T. Kentischer, W. Schmidt, and T. Udem. Laser frequency combs for astronomical observations. *Science*, 321 (5894), **2008**, 1335–7. DOI: 10.1126/science.1161030 (cited on page 1).

[13] B. R. Washburn, S. A. Diddams, N. R. Newbury, J. W. Nicholson, M. F. Yan, and C. G. Jørgensen. Phase-locked, erbium-fiber-laser-based frequency comb in the near infrared. *Optics Letters*, 29 (3), **2004**, 250–252. DOI: 10.1364/OL.29.000250 (cited on page 1).

[14] C. Gohle, T. Udem, M. Herrmann, J. Rauschenberger, R. Holzwarth, H. A. Schuessler, F. Krausz, and T. W. Hänsen. A frequency comb in the extreme ultraviolet. *Nature*, 436 (7048), **2005**, 234–237. DOI: 10.1038/nature03851 (cited on page 1).

[15] S. A. Diddams. The evolving optical frequency comb [Invited]. *Journal of the Optical Society of America B*, 27 (11), **2010**, B51–B62. DOI: 10.1364/JOSAB.27.000B51 (cited on page 1).

[16] J. Faist, G. Villares, G. Scalari, M. Rosch, C. Bonzon, A. Hugi, and M. Beck. Quantum Cascade Laser Frequency Combs. *Nanophotonics*, 5 (2), **2016**, 272–291. DOI: 10.1515/nanoph-2016-0015. arXiv: 1510.09075 (cited on page 1).

[17] D. T. Spencer, T. Drake, T. C. Briles, J. Stone, L. C. Sinclair, C. Fredrick, Q. Li, D. Westly, B. R. Ilic, A. Bluestone, N. Volet, T. Komljenovic, L. Chang, S. H. Lee, D. Y. Oh, T. J. Kippenberg, E. Norberg, L. Theogarajan, M.-g. Suh, K. Y. Yang, H. P. Martin, K. Vahala, N. R. Newbury, K. Srinivasan, J. E. Bowers, S. A. Diddams, and S. B. Papp. An optical-frequency synthesizer using integrated photonics. *Nature*, 557, **2018**, 81–85. DOI: 10.1038/s41586-018-0065-7 (cited on page 2).

[18] R. W. Boyd. **Nonlinear Optics**. San Diego, CA: Elsevier, 2003 (cited on page 6).

[19] T. M. Fortier, D. J. Jones, and S. T. Cundiff. Phase stabilization of an octave-spanning Ti:sapphire laser. *Opt. Lett.*, 28 (22), **2003**, 2198–2200. DOI: 10.1364/OL.28.002198 (cited on page 7).

[20] D. R. Carlson, D. D. Hickstein, A. Lind, S. Droste, D. Westly, N. Nader, I. Coddington, N. R. Newbury, K. Srinivasan, S. A. Diddams, and S. B. Papp. Self-referenced frequency combs using high-efficiency silicon-nitride waveguides. 42 (12), **2017**, 2314–2317. DOI: 10.1364/OL.42.002314. arXiv: 1704.03909 (cited on page 7).

[21] P Del'Haye, A Schliesser, O Arcizet, T Wilken, R Holzwarth, and T. J. Kippenberg. Optical frequency comb generation from a monolithic microresonator. *Nature*, 450 (7173), **2007**, 1214–1217. DOI: 10.1038/nature06401.

[22] T. J. Kippenberg, R Holzwarth, and S. A. Diddams. Microresonator-Based Optical Frequency Combs. *Science (New York, N.Y.)*, 332 (6029), **2011**, 555–559. DOI: 10.1126/science.1193968.

[23] A. A. Savchenkov, A. B. Matsko, and L Maleki. On Frequency Combs in Monolithic Resonators. *Nanophotonics*, 5, **2016**, 363–391. DOI: 10.1515/nanoph-2016-0031.

[24] Y. K. Chembo. Kerr optical frequency combs: Theory, applications and perspectives. *Nanophotonics*, 5 (2), **2016**, 214–230. DOI: 10.1515/nanoph-2016-0013.

[25] A. Pasquazi, M. Peccianti, L. Razzari, D. J. Moss, S. Coen, M. Erkintalo, Y. K. Chembo, T. Hansson, S. Wabnitz, P. Del'Haye, X. Xue, A. M. Weiner, and R. Morandotti. Micro-combs: A novel generation of optical sources. *Physics Reports*, 729, **2017**, 1–81. DOI: 10.1016/j.physrep.2017.08.004.

[26] H. Lee, T. Chen, J. Li, K. Y. Yang, S. Jeon, O. Painter, and K. J. Vahala. Chemically etched ultrahigh-Q wedge-resonator on a silicon chip. *Nature Photonics*, 6 (6), **2012**, 369–373. DOI: 10.1038/nphoton.2012.109. arXiv: 1112.2196.

[27] X. Yi, Q.-F. Yang, K. Y. Yang, M.-G. Suh, and K. Vahala. Soliton frequency comb at microwave rates in a high-Q silica microresonator. *Optica*, 2 (12), **2015**, 1078–1085.

[28] P. Del'Haye, S. A. Diddams, and S. B. Papp. Laser-machined ultra-high-Q microrod resonators for nonlinear optics. *Applied Physics Letters*, 102, **2013**, 221119.

[29] W Liang, A. A. Savchenkov, A. B. Matsko, V. S. Ilchenko, D Seidel, and L Maleki. Generation of near-infrared frequency combs from a MgF$_2$ whispering gallery mode resonator. *Optics Letters*, 36 (12), **2011**, 2290–2292. DOI: 10.1364/OL.36.002290.

[30] A. a. Savchenkov, A. B. Matsko, V. S. Ilchenko, I. Solomatine, D. Seidel, and L. Maleki. Tunable optical frequency comb with a crystalline whispering gallery mode resonator. *Physical Review Letters*, 101 (9), **2008**, 1–4. DOI: 10.1103/PhysRevLett.101.093902. arXiv: 0804.0263.

[31] Y. Okawachi, K. Saha, J. S. Levy, Y. H. Wen, M. Lipson, and A. L. Gaeta. Octave-spanning frequency comb generation in a silicon nitride chip. *Optics Letters*, 36 (17), **2011**, 3398–3400. DOI: 10.1364/OL.36.003398. arXiv: 1107.5555.

[32] D. J. Moss, R Morandotti, A. L. Gaeta, and M Lipson. New CMOS-compatible platforms based on silicon nitride and Hydex for nonlinear optics. *Nature Photonics*, 7 (July), **2013**, 597–607. DOI: 10.1038/nphoton.2013.183.

[33] D. Braje, L. Hollberg, and S. Diddams. Brillouin-Enhanced Hyperparametric Generation of an Optical Frequency Comb in a Monolithic Highly Nonlinear Fiber Cavity Pumped by a cw Laser. *Physical Review Letters*, 102 (19), **2009**, 193902. DOI: 10.1103/PhysRevLett.102.193902.

[34] E. Obrzud, S. Lecomte, and T. Herr. Temporal solitons in microresonators driven by optical pulses. *Nature Photonics*, 11 (August), **2017**, 600–607. DOI: 10.1038/nphoton.2017.140. arXiv: 1612.08993.

[35] V. S. Ilchenko and A. B. Matsko. Optical resonators with whispering-gallery modes - Part II: Applications. *IEEE Journal on Selected Topics in Quantum Electronics*, 12 (1), **2006**, 15–32. DOI: 10.1109/JSTQE.2005.862943.

[36] K. Y. Yang, K. Beha, D. C. Cole, X. Yi, P. Del'Haye, H. Lee, J. Li, D. Y. Oh, S. A. Diddams, S. B. Papp, and K. J. Vahala. Broadband dispersion-engineered microresonator on a chip. *Nature Photonics*, 10 (March), **2016**, 316–320. DOI: 10.1038/nphoton.2016.36.

[37] G. P. Agrawal. **Nonlinear Fiber Optics**. 4th. Burlington, MA: Elsevier, 2007 (cited on page 13).

[38] M. L. Calvo and V. Lakshminarayanan, eds. **Optical Waveguides: From Theory to Applied Technologies**. Boca Raton, FL: Taylor & Francis, 2007.

[39] A. N. Oraevsky. Whispering-gallery waves. *Quantum Electronics*, 32 (42), **2002**, 377–400. DOI: 10.1070/QE2001v031n05ABEH002205. arXiv: arXiv:1011.1669v3.

[40] H. A. Haus. **Waves and Fields in Optoelectronics**. Englewood Cliffs: Prentice-Hall, 1984.

[41] J. C. Knight, G. Cheung, F. Jacques, and T. A. Birks. Phase-matched excitation of whispering-gallery-mode resonances by a fiber taper. *Optics Letters*, 22 (15), **1997**, 1129. DOI: 10.1364/OL.22.001129.

[42] S. M. Spillane, T. J. Kippenberg, O. J. Painter, and K. J. Vahala. Ideality in a Fiber-Taper-Coupled Microresonator System for Application to Cavity Quantum Electrodynamics. *Physical review letters*, 91 (4), **2003**, 043902. DOI: 10.1103/PhysRevLett.91.043902.

[43] E. Shah Hosseini, S. Yegnanarayanan, A. H. Atabaki, M. Soltani, and A. Adibi. Systematic design and fabrication of high-Q single-mode pulley-coupled planar silicon nitride microdisk resonators at visible wavelengths. *Optics Express*, 18 (3), **2010**, 2127. DOI: 10.1364/OE.18.002127.

[44] T. Carmon, L. Yang, and K. J. Vahala. Dynamical thermal behavior and thermal self-stability of microcavities. *Optics Express*, 12 (20), **2004**, 4742–4750. URL: http://www.ncbi.nlm.nih.gov/pubmed/19484026http://www.opticsinfobase.org/oe/abstract.cfm?uri=oe-12-20-4742.

[45] R. del Coso and J. Solis. Relation between nonlinear refractive index and third-order susceptibility in absorbing media. *Journal of the Optical Society of America B*, 21 (3), **2004**, 640. DOI: 10.1364/JOSAB.21.000640.

[46] T. Kippenberg, S. Spillane, and K. Vahala. Kerr-Nonlinearity Optical Parametric Oscillation in an Ultrahigh-Q Toroid Microcavity. *Physical Review Letters*, 93 (8), **2004**, 083904. DOI: 10.1103/PhysRevLett.93.083904.

[47] A. A. Savchenkov, A. B. Matsko, D. Strekalov, M. Mohageg, V. S. Ilchenko, and L. Maleki. Low threshold optical oscillations in a whispering gallery mode CaF 2 resonator. *Physical Review Letters*, 93 (24), **2004**, 2–5. DOI: 10.1103/PhysRevLett.93.243905.

[48] I. H. Agha, Y. Okawachi, M. A. Foster, J. E. Sharping, and A. L. Gaeta. Four-wave-mixing parametric oscillations in dispersion-compensated high- Q silica microspheres. *Physical Review A - Atomic, Molecular, and Optical Physics*, 76 (4), **2007**, 1–4. DOI: 10.1103/PhysRevA.76.043837.

[49] T. Herr, V. Brasch, J. D. Jost, C. Y. Wang, N. M. Kondratiev, M. L. Gorodetsky, and T. J. Kippenberg. Temporal solitons in optical microresonators. *arXiv*, **2012**, 1211.0733. DOI: 10.1038/nphoton.2013.343. arXiv: 1211.0733.

[50] T. Herr, V. Brasch, J. D. Jost, C. Y. Wang, N. M. Kondratiev, M. L. Gorodetsky, and T. J. Kippenberg. Temporal solitons in optical microresonators. *Nature Photonics*, 8 (2), **2014**, 145–152. DOI: 10.1109/CLEOE-IQEC.2013.6801769. arXiv: 1211.0733.

[51] F. Leo, S. Coen, P. Kockaert, S.-P. Gorza, P. Emplit, and M. Haelterman. Temporal cavity solitons in one-dimensional Kerr media as bits in an all-optical buffer. *Nature Photonics*, 4 (7), **2010**, 471–476. DOI: 10.1038/nphoton.2010.120.

[52] T. Herr, K. Hartinger, J. Riemensberger, C. Y. Wang, E. Gavartin, R. Holzwarth, M. L. Gorodetsky, and T. J. Kippenberg. Universal formation dynamics and noise of Kerr-frequency combs in microresonators. *Nature Photonics*, 6 (7), **2012**, 480–487. DOI: 10.1038/nphoton.2012.127.

[53] Y. K. Chembo and C. R. Menyuk. Spatiotemporal Lugiato-Lefever formalism for Kerr-comb generation in whispering-gallery-mode resonators. *Physical Review A*, 87, **2013**, 053852. DOI: 10.1103/PhysRevA.87.053852.

[54] S. Coen, H. G. Randle, T. Sylvestre, and M. Erkintalo. Modeling of octave-spanning Kerr frequency combs using a generalized mean-field Lugiato-Lefever model. *Optics letters*, 38 (1), **2013**, 37–39. URL: http://www.ncbi.nlm.nih.gov/pubmed/23282830.

[55] M. Haelterman, S. Trillo, and S. Wabnitz. Dissipative modulation instability in a nonlinear dispersive ring cavity. *Optics Communications*, 91 (5-6), **1992**, 401–407. DOI: 10.1016/0030-4018(92)90367-Z.

[56] T Hansson, M Bernard, and S Wabnitz. Modulational Instability of Nonlinear Polarization Mode Coupling in Microresonators. 35 (4), **2018**. URL: https://arxiv.org/pdf/1802.04535.pdf. arXiv: arXiv:1802.04535v1.

[57] Y. K. Chembo, I. S. Grudinin, and N Yu. Spatiotemporal dynamics of Kerr-Raman optical frequency combs. *Physical Review A*, 92 (4), **2015**, 4. DOI: 10.1103/PhysRevA.92.043818.

[58] C. Godey, I. V. Balakireva, A. Coillet, and Y. K. Chembo. Stability analysis of the spatiotemporal Lugiato-Lefever model for Kerr optical frequency combs in the anomalous and normal dispersion regimes. *Physical Review A*, 89 (6), **2014**, 063814. DOI: 10.1103/PhysRevA.89.063814.

[59] I. V. Barashenkov and Y. S. Smirnov. Existence and stability chart for the ac-driven, damped nonlinear Schrödinger solitons. *Physical Review E - Statistical Physics, Plasmas, Fluids, and Related Interdisciplinary Topics*, 54 (5), **1996**, 5707–5725. DOI: 10.1103/PhysRevE.54.5707.

[60] A Coillet and Y. K. Chembo. Routes to spatiotemporal chaos in Kerr optical frequency combs. *Chaos*, 24 (1), **2014**, 5. DOI: 10.1063/1.4863298. arXiv: arXiv:1401.0927v1.

[61] L. A. Lugiato and R Lefever. Spatial Dissipative Structures in Passive Optical Systems. *Physical Review Letters*, 58 (21), **1987**, 2209–2211.

[62] L. Lugiato and R Lefever. Diffraction stationary patterns in passive optical systems. *Interaction of Radiation with Matter*, **1987**.

[63] W. H. Renninger and P. T. Rakich. Closed-form solutions and scaling laws for Kerr frequency combs. *Scientific Reports*, 6 (1), **2016**, 24742. DOI: 10.1038/srep24742. arXiv: 1412.4164.

[64] J. S. Russell. Report on Waves. *Fourteenth meeting of the British Association for the Advancement of Science*, **1844**, 311–390.

[65] M. Brambilla, L. A. Lugiato, F. Prati, L. Spinelli, and W. J. Firth. Spatial soliton pixels in semiconductor devices. *Physical Review Letters*, 79 (11), **1997**, 2042–2045. DOI: 10.1103/PhysRevLett.79.2042.

[66] S. Minardi, F. Eilenberger, Y. V. Kartashov, A. Szameit, U. Röpke, J. Kobelke, K. Schuster, H. Bartelt, S. Nolte, L. Torner, F. Lederer, A. Tünnermann, and T. Pertsch. Three-dimensional light bullets in arrays of waveguides. *Physical Review Letters*, 105 (26), **2010**, 1–4. DOI: 10.1103/PhysRevLett.105.263901. arXiv: 1101.0734.

[67] F. X. Kärtner, I. D. Jung, and U. Keller. Soliton mode-locking with saturable absorbers. *IEEE Journal on Selected Topics in Quantum Electronics*, 2 (3), **1996**, 540–556. DOI: 10.1109/2944.571754.

[68] P. Grelu and N. Akhmediev. Dissipative solitons for mode-locked lasers. *Nature Photonics*, 6 (February), **2012**, 84–92. DOI: 10.1109/PGC.2010.5706017.

[69] L. F. Mollenauer and J. P. Gordon. **Solitons in Optical Fibers**. Academic Press, 2006, p. 296.

[70] A. Hasegawa and Y. Kodama. **Solitons in Optical Communications**. Academic Press, 1995.

[71] H. A. Haus and W. S. Wong. Solitons in optical communications. *Reviews of Modern Physics*, 68 (2), **1996**, 423–444. DOI: 10.1103/RevModPhys.68.423.

[72] S. Coen and M. Erkintalo. Universal scaling laws of Kerr frequency combs. *Optics letters*, 38 (11), **2013**, 1790–1792. DOI: 10.1364/OL.38.001790. arXiv: arXiv:1303.7078v1.

[73] H. Guo, M. Karpov, E. Lucas, A. Kordts, M. H. Pfeiffer, V. Brasch, G. Lihachev, V. E. Lobanov, M. L. Gorodetsky, and T. J. Kippenberg. Universal dynamics and deterministic switching of dissipative Kerr solitons in optical microresonators. *Nature Physics*, 13 (1), **2017**, 94–102. DOI: 10.1038/nphys3893. arXiv: 1601.05036.

[74] N. J. Zabusky and M. D. Kruskal. Interaction of "solitons" in a collisionless plasma and the recurrence of initial states. *Physical Review Letters*, 15 (6), **1965**, 240.

[75] J. P. Gordon. Interaction forces among solitons in optical fibers. *Optics Letters*, 8 (11), **1983**, 596. DOI: 10.1364/OL.8.000596.

[76] B. A. Malomed. Bound solitons in the nonlinear Schrodinger-Ginzburg-Landau equation. *Physical Review A*, 44 (10), **1991**, 6954–6957. DOI: 10.1103/PhysRevA.44.6954.

[77] J. K. Jang, M Erkintalo, S. G. Murdoch, and S Coen. Ultraweak long-range interactions of solitons observed over astronomical distances. *Nature Photonics*, 7 (8), **2013**, 657–663. DOI: 10.1038/nphoton.2013.157. arXiv: arXiv:1305.6670v1.

[78] P. Parra-Rivas, D. Gomila, P. Colet, and L. Gelens. Interaction of solitons and the formation of bound states in the generalized Lugiato-Lefever equation. *European Physical Journal D*, 71 (7), **2017**, 198. DOI: 10.1140/epjd/e2017-80127-5. arXiv: arXiv:1705.02619v1.

[79] Y. Wang, F. Leo, J. Fatome, M. Erkintalo, S. G. Murdoch, and S. Coen. Universal mechanism for the binding of temporal cavity solitons, **2017**, 1–10. URL: http://arxiv.org/abs/1703.10604. arXiv: 1703.10604.

[80] V. Brasch, T. Herr, M. Geiselmann, G. Lihachev, M. H. P. Pfeiffer, M. L. Gorodetsky, and T. J. Kippenberg. Photonic chip-based optical frequency comb using soliton Cherenkov radiation. *Science*, 351 (6271), **2016**, 357. DOI: 10.1364/CLEO_SI.2015.STh4N.1. arXiv: 1410.8598.

[81] J. R. Stone, T. C. Briles, T. E. Drake, D. T. Spencer, D. R. Carlson, S. A. Diddams, and S. B. Papp. Thermal and Nonlinear Dissipative-Soliton Dynamics in Kerr Microresonator Frequency Combs. *arXiv*, **2017**, 1708.08405. URL: http://arxiv.org/abs/1708.08405. arXiv: 1708.08405.

[82] V. E. Lobanov, G. V. Lihachev, N. G. Pavlov, A. V. Cherenkov, T. J. Kippenberg, and M. L. Gorodetsky. Harmonization of chaos into a soliton in Kerr frequency combs. *Optics Express*, 24 (24), **2016**, 27382. DOI: 10.1126/science.aah4243. arXiv: 1607.08222.

[83] C. Joshi, J. K. Jang, K. Luke, X. Ji, S. A. Miller, A. Klenner, Y. Okawachi, M. Lipson, and A. L. Gaeta. Thermally controlled comb generation and soliton modelocking in microresonators. *Optics Letters*, 41 (11), **2016**, 2565–2568. DOI: 10.1364/OL.41.002565. arXiv: 1603.08017.

[84] W. Wang, Z. Lu, W. Zhang, S. T. Chu, B. E. Little, L. Wang, X. Xie, M. Liu, Q. Yang, L. Wang, J. Zhao, G. Wang, Q. Sun, Y. Liu, Y. Wang, and W. Zhao. Robust soliton crystals in a thermally controlled microresonator. *Optics Letters*, 43 (9), **2018**, 2002–2005. DOI: 10.1364/OL.43.002002.

[85] J. K. Jang, M. Erkintalo, S. G. Murdoch, and S. Coen. Writing and erasing of temporal cavity solitons by direct phase modulation of the cavity driving field. *Optics Letters*, 40 (20), **2015**, 4755–4758. DOI: 10.1364/OL.40.004755. arXiv: 1501.05289.

[86] J. K. Jang, M. Erkintalo, S. Coen, and S. G. Murdoch. Temporal tweezing of light through the trapping and manipulation of temporal cavity solitons. *Nature Communications*, 6, **2015**, 7370. DOI: 10.1038/ncomms8370. arXiv: 1410.4836.

[87] Y. Wang, B. Garbin, F. Leo, S. Coen, M. Erkintalo, and S. G. Murdoch. Writing and Erasure of Temporal Cavity Solitons via Intensity Modulation of the Cavity Driving Field. *arXiv*, **2018**, 1802.07428. arXiv: 1802.07428.

[88] S. B. Papp, K. Beha, P. Del'Haye, F. Quinlan, H. Lee, K. J. Vahala, and S. A. Diddams. Microresonator frequency comb optical clock. *Optica*, 1 (1), **2014**, 10–14. DOI: 10.1364/OPTICA.1.000010. arXiv: 1309.3525.

[89] M. G. Suh, Q. F. Yang, K. Y. Yang, X. Yi, and K. J. Vahala. Microresonator soliton dual-comb spectroscopy. *Science*, 354 (6312), **2016**, 1–5. DOI: 10.1126/science.aah6516. arXiv: 1607.08222.

[90] P. Marin-Palomo, J. N. Kemal, M. Karpov, A. Kordts, J. Pfeifle, M. H. Pfeiffer, P. Trocha, S. Wolf, V. Brasch, M. H. Anderson, R. Rosenberger, K. Vijayan, W. Freude, T. J. Kippenberg, and C. Koos. Microresonator-based solitons for massively parallel coherent optical communications. *Nature*, 546 (7657), **2017**, 274–279. DOI: 10.1038/nature22387. arXiv: 1610.01484.

[91] J. D. Jost, T. Herr, C. Lecaplain, V. Brasch, M. H. P. Pfeiffer, and T. J. Kippenberg. Counting the cycles of light using a self-referenced optical microresonator. *Optica*, 2 (8), **2015**, 706–711. DOI: 10.1364/OPTICA.2.000706. arXiv: 1411.1354.

[92] P. Del'Haye, A. Coillet, T. Fortier, K. Beha, D. C. Cole, K. Y. Yang, H. Lee, K. J. Vahala, S. B. Papp, and S. A. Diddams. Phase-coherent microwave-to-optical link with a self-referenced microcomb. *Nature Photonics*, 10 (June), **2016**, 1–5. DOI: 10.1038/nphoton.2016.105.

[93] V. Brasch, E. Lucas, J. D. Jost, M. Geiselmann, and T. J. Kippenberg. Self-referenced photonic chip soliton Kerr frequency comb. *Light: Science & Applications*, 6 (1), **2017**, e16202. DOI: 10.1038/lsa.2016.202. arXiv: 1605.02801.

[94] T. C. Briles, J. R. Stone, T. E. Drake, D. T. Spencer, C. Frederick, Q. Li, D. A. Westly, B. R. Illic, K. Srinivasan, S. A. Diddams, and S. B. Papp. Kerr-microresonator solitons for accurate carrier-envelope-frequency stabilization. *arXiv*, **2017**, 1711.06251. URL: http://arxiv.org/abs/1711.06251. arXiv: 1711.06251.

[95] H. Taheri, A. A. Eftekhar, K. Wiesenfeld, and A. Adibi. Soliton formation in whispering-gallery-mode resonators via input phase modulation. *IEEE Photonics Journal*, 7 (2), **2015**, 2200309. DOI: 10.1109/JPHOT.2015.2416121.

[96] M. Zajnulina, M. Böhm, D. Bodenmüller, K. Blow, J. C. Boggio, A. Rieznik, and M. Roth. Characteristics and stability of soliton crystals in optical fibres for the purpose of optical frequency comb generation. *Optics Communications*, 393 (November 2016), **2017**, 95–102. DOI: 10.1016/j.optcom.2017.02.035.

[97] A. Haboucha, H. Leblond, M. Salhi, A. Komarov, and F. Sanchez. Coherent soliton pattern formation in a fiber laser. *Optics Letters*, 33 (5), **2008**, 524–526. DOI: 10.1364/OL.33.000524.

[98] F. Amrani, M. Salhi, P. Grelu, H. Leblond, and F. Sanchez. Universal soliton pattern formations in passively mode-locked fiber lasers. *Optics letters*, 36 (9), **2011**, 1545–1547. DOI: 10.1364/OL.36.001545.

[99] A. Haboucha, H. Leblond, M. Salhi, A. Komarov, and F. Sanchez. Analysis of soliton pattern formation in passively mode-locked fiber lasers. *Physical Review A*, 78, **2008**, 043806. DOI: 10.1103/PhysRevA.78.043806.

[100] B. A. Malomed, A Schwache, and F Mitschke. Soliton lattice and gas in passive fiber-ring resonators. *Fiber and Integrated Optics*, 17 (4), **1998**, 267–277. DOI: 10.1080/014680398244867.

[101] F. Mitschke and A. Schwache. Soliton ensembles in a nonlinear resonator. *Journal of Optics B: Quantum and Semiclassical Optics*, 10 (6), **1998**, 779–788.

[102] A. Schwache and F. Mitschke. Properties of an optical soliton gas. *Physical Review E*, 55 (6), **1997**, 7720–7725. DOI: 10.1103/PhysRevE.55.7720.

[103] H. A. Haus and W. Huang. Coupled-Mode Theory. *Proceedings of the IEEE*, 79 (10), **1991**, 1505–1518. DOI: 10.1109/5.104225.

[104] A. A. Savchenkov, A. B. Matsko, W Liang, V. S. Ilchenko, D Seidel, and L Maleki. Kerr frequency comb generation in overmoded resonators. *Opt Express*, 20 (24), **2012**, 27290–27298. DOI: 10.1364/OE.20.027290\r10.1364/OE.20.027290.. arXiv: arXiv:1201.1959v1.

[105] T. Herr, V. Brasch, J. D. Jost, I. Mirgorodskiy, G. Lihachev, M. L. Gorodetsky, and T. J. Kippenberg. Mode Spectrum and Temporal Soliton Formation in Optical Microresonators. *Physical Review Letters*, 113 (12), **2014**, 123901. DOI: 10.1103/PhysRevLett.113.123901.

[106] Y. Liu, Y. Xuan, X. Xue, P.-H. Wang, S. Chen, A. J. Metcalf, J. Wang, D. E. Leaird, M. Qi, and A. M. Weiner. Investigation of mode coupling in normal-dispersion silicon nitride microresonators for Kerr frequency comb generation. *Optica*, 1 (3), **2014**, 137–144. DOI: 10.1364/OPTICA.1.000137.

[107] X. Xue, Y. Xuan, Y. Liu, P.-H. Wang, S. Chen, J. Wang, D. E. Leaird, M. Qi, and A. M. Weiner. Mode-locked dark pulse Kerr combs in normal-dispersion microresonators. *Nat Photon*, 9 (9), **2015**, 594–600. DOI: 10.1038/nphoton.2015.137.

[108] C. Bao, Y. Xuan, D. E. Leaird, S. Wabnitz, M. Qi, and A. M. Weiner. Spatial mode-interaction induced single soliton generation in microresonators. *Optica*, 4 (9), **2017**, 1011. DOI: 10.1364/OPTICA.4.001011.

[109] T. Hansson and S. Wabnitz. Bichromatically pumped microresonator frequency combs. *Physical Review A*, 90, **2014**, 013811. DOI: 10.1103/PhysRevA.90.013811. arXiv: 1404.2792.

[110] D. V. Skryabin and W. J. Firth. Interaction of cavity solitons in degenerate optical parametric oscillators. *Optics letters*, 24 (15), **1999**, 1056–1058. DOI: 10.1364/OL.24.001056. arXiv: 9906004 [patt-sol].

[111] S. Wabnitz. Control of soliton train transmission, storage, and clock recovery by cw light injection. *Journal of the Optical Society of America B*, 13 (12), **1996**, 2739–2749. URL: http://www.scopus.com/inward/record.url?eid=2-s2.0-0030378988{\&}partnerID=tZOtx3y1.

[112] J. A. Barker and D. Henderson. What is "liquid"? Understanding the states of matter. *Reviews of Modern Physics*, 48 (4), **1976**, 587–671. DOI: 10.1103/RevModPhys.48.587.

[113] T. Egami and S. Billinge. **Underneath the Bragg Peaks**. 2nd. Oxford, UK: Elsevier, 2012, p. 422.

[114] N. W. Ashcroft and D. N. Mermin. **Solid State Physics**. 1st ed. Belmont, CA: Brooks/Cole, 1976, p. 826.

[115] A. Weiner. **Ultrafast Optics**. 1st ed. Hoboken, NJ: Wiley, 2009, p. 598.

[116] T. Kobayashi, T. Sueta, Y. Cho, and Y. Matsuo. High-repetition-rate optical pulse generator using a Fabry-Perot electro-optic modulator. *Applied Physics Letters*, 21 (8), **1972**, 341–343. DOI: 10.1063/1.1654403.

[117] M. Kourogi, K. Nakagawa, and M. Ohtsu. Wide-Span Optical Frequency Comb Generator for. 29 (10), **1993**.

[118] H. Murata, A. Morimoto, T. Kobayashi, and S. Yamamoto. Optical pulse generation by electrooptic-modulation method and its application to integrated ultrashort pulse generators. *IEEE Journal of Selected Topics in Quantum Electronics*, 6 (6), **2000**, 1325–1331. DOI: 10.1109/2944.902186.

[119] T. Sakamoto, T. Kawanishi, and M. Izutsu. Asymptotic formalism for ultraflat optical frequency comb generation using a Mach-Zehnder modulator. *Optics letters*, 32 (11), **2007**, 1515–1517. DOI: 10.1364/OL.32.001515.

[120] I. Morohashi, T. Sakamoto, H. Sotobayashi, T. Kawanishi, I. Hosako, and M. Tsuchiya. Widely repetition-tunable 200 fs pulse source using a Mach-Zehnder-modulator-based flat comb generator and dispersion-flattened dispersion-decreasing fiber. *Optics letters*, 33 (11), **2008**, 1192–1194. DOI: 10.1364/OL.33.001192.

[121] A. Ishizawa, T. Nishikawa, A. Mizutori, H. Takara, S. Aozasa, A. Mori, H. Nakano, A. Takada, and M. Koga. Octave-spanning frequency comb generated by 250 fs pulse train emitted from 25 GHz externally phase-modulated laser diode for carrier-envelope-offset-locking. *Electronics Letters*, 46 (19), **2010**, 1343. DOI: 10.1049/el.2010.2228.

[122] R. Wu, V. R. Supradeepa, C. M. Long, D. E. Leaird, and A. M. Weiner. Generation of very flat optical frequency combs from continuous-wave lasers using cascaded intensity and phase modulators driven by tailored radio frequency waveforms. *Optics Letters*, 35 (19), **2010**, 3234. DOI: 10.1364/OL.35.003234. arXiv: 1005.5373.

[123] V. R. Supradeepa and A. M. Weiner. Bandwidth scaling and spectral flatness enhancement of optical frequency combs from phase-modulated continuous-wave lasers using cascaded four-wave mixing. *Optics Letters*, 37 (15), **2012**, 3066. DOI: 10.1364/OL.37.003066.

[124] A. J. Metcalf, V. Torres-company, D. E. Leaird, S. Member, A. M. Weiner, and A. Broadband. High-Power Broadly Tunable Electrooptic Frequency Comb Generator. *IEEE Journal of Selected Topics in Quantum Electronics*, 19 (6), **2013**, 3500306. URL: http://ieeexplore.ieee.org/stamp/stamp.jsp?arnumber=06553388.

[125] R. Wu, V. Torres-company, D. E. Leaird, and A. M. Weiner. Optical Frequency Comb Generation. 21 (5), **2013**, 6045–6052. DOI: 10.1364/OE.21.006045.

[126] J. M. Dudley, G. G. Genty, and S. Coen. Supercontinuum generation in photonic crystal fiber. *Reviews of Modern Physics*, 78 (4), **2006**, 1135–1184. DOI: 10.1103/RevModPhys.78.1135.

[127] A. M. Weiner. Femtosecond pulse shaping using spatial light modulators. *Review of Scientific Instruments*, 71 (5), **2000**, 1929–1960. DOI: 10.1063/1.1150614.

[128] K. Beha, D. C. Cole, P. Del'Haye, A. Coillet, S. A. Diddams, and S. B. Papp. Electronic synthesis of light. *Optica*, 4 (4), **2017**, 406–411. DOI: 10.1364/OPTICA.4.000406.

[129] a. a. Amorim, M. V. Tognetti, P Oliveira, J. L. Silva, L. M. Bernardo, F. X. Kärtner, and H. M. Crespo. Sub-two-cycle pulses by soliton self-compression in highly nonlinear photonic crystal fibers. *Optics letters*, 34 (24), **2009**, 3851–3853. DOI: 10.1364/OL.34.003851.

[130] G. Di Domenico, S. Schilt, and P. Thomann. Simple approach to the relation between laser frequency noise and laser line shape. *Applied optics*, 49 (25), **2010**, 4801–4807. DOI: 10.1364/AO.49.004801.

[131] D. R. Carlson, D. D. Hickstein, D. C. Cole, S. A. Diddams, and S. B. Papp. Dual-comb interferometry via repetition-rate switching of a single frequency comb. *arXiv*, **2018**, 1806.05311. URL: http://arxiv.org/abs/1806.05311. arXiv: 1806.05311.

[132] A. J. Metcalf, C. Bender, S. Blakeslee, W. Brand, D. Carlson, S. A. Diddams, C. Fredrick, S. Halverson, F. Hearty, D. Hickstein, J. Jennings, S. Kanodia, K. Kaplan, E. Lubar, S. Mahadevan, A. Monson, J. Ninan, C. Nitroy, S. Papp, L. Ramsey, P. Robertson, A. Roy, C. Schwab, K. Srinivasan, G. K. Stefansson, and R. Terrien. Infrared Astronomical Spectroscopy for Radial Velocity Measurements with 10 cm/s Precision. In: **Conference on Lasers and Electro-Optics**. 2018, JTh5A.1.

[133] S. Backus, C. G. Durfee, M. M. Murnane, and H. C. Kapteyn. High power ultrafast lasers. *Review of Scientific Instruments*, 69 (3), **1998**, 1207. DOI: 10.1063/1.1148795.

[134] A. Baltuska, M. Uiberacker, E. Goulielmakis, R. Kienberger, V. S. Yakovlev, T. Udem, T. W. Hänsch, and F. Krausz. Phase-Controlled Amplification of Few-Cycle Laser Pulses. *IEEE Journal of Selected Topics in Quantum Electronics*, 9 (4), **2003**, 972–989.

[135] C. Gohle, J. Rauschenberger, T. Fuji, T. Udem, A. Apolonski, F. Krausz, and T. W. Hänsch. Carrier envelope phase noise in stabilized amplifier systems. 30 (18), **2005**, 2487–2489.

[136] J. Rauschenberger, T. Fuji, M. Hentschel, A.-J. Verhoef, T. Udem, C. Gohle, T. W. Hänsch, and F. Krausz. Carrier-envelope phase-stabilized amplifier system. *Laser Physics Letters*, 3 (1), **2006**, 37–42. DOI: 10.1002/lapl.200510053.

[137] M. E. Fermann, V. I. Kruglov, B. C. Thomsen, J. M. Dudley, and J. D. Harvey. Self-similar propagation and amplification of parabolic pulses in optical fibers. *Physical review letters*, 84 (26 Pt 1), **2000**, 6010–3. URL: http://www.ncbi.nlm.nih.gov/pubmed/10991111.

[138] M. Hirano, T. Nakanishi, T. Okuno, and M. Onishi. Silica-Based Highly Nonlinear Fibers and Their Application. *Sel. Top. Quantum Electron.*, 15 (1), **2009**, 103–113. DOI: 10.1109/JSTQE.2008.2010241 (cited on page 13).

[139] D. Mandridis, I. Ozdur, F. Quinlan, M. Akbulut, J. J. Plant, P. W. Juodawlkis, and P. J. Delfyett. Low-noise, low repetition rate, semiconductor-based mode-locked laser source suitable for high bandwidth photonic analog – digital conversion. *Applied Optics*, 49 (15), **2010**, 2850–2857.

[140] H.-A. Bachor and P. J. Manson. Practical Implications of Quantum Noise. *Journal of Modern Optics*, 37 (11), **1990**, 1727–1740. DOI: 10.1080/09500349014551951.

[141] F. Quinlan, T. M. Fortier, H. Jiang, and S. a. Diddams. Analysis of shot noise in the detection of ultrashort optical pulse trains. *Journal of the Optical Society of America B*, 30 (6), **2013**, 1775. DOI: 10.1364/JOSAB.30.001775.

[142] D. C. Cole, K. M. Beha, S. A. Diddams, and S. B. Papp. Octave-spanning supercontinuum generation via microwave frequency multiplication. *Proceedings of the 8th Sympsion on Frequency Standards and Metrology 2015, Journal of Physics: Conference Series*, 723, **2016**, 012035. DOI: 10.1088/1742-6596/723/1/012035.

[143] A. M. Heidt. Efficient Adaptive Step Size Method for the Simulation of Supercontinuum Generation in Optical Fibers. *Journal of Lightwave Technology*, 27 (18), **2009**, 3984–3991 (cited on pages 9, 10).

[144] J. Hult. A Fourth-Order Runge-Kutta in the Interaction Picture Method for Simulating Supercontinuum Generation in Optical Fibers. *Journal of Lightwave Technology*, 25 (12), **2007**, 3770–3775. DOI: 10.1109/JLT.2007.909373 (cited on pages 9, 10, 13).

[145] R. Driad, J. Rosenzweig, R. E. Makon, R. Lösch, V. Hurm, H. Walcher, and M. Schlechtweg. InP DHBT-Based IC Technology for 100-Gb / s Ethernet. *IEEE Trans. on Electron. Devices*, 58 (8), **2011**, 2604–2609.

[146] D. Ferenci, M. Grozing, M. Berroth, R. Makon, R. Driad, and J. Rosenzweig. A 25 GHz Analog Demultiplexer with a Novel Track and Hold Circuit for a 50 GS / s A / D-Conversion System in InP DHBT Technology. In: **Microwave Symposium Digest**. 2012, pp. 1–3.

[147] K. J. Blow and D Wood. Theoretical description of transient stimulated Raman scattering in optical fibers. *Quantum Electronics, IEEE Journal of*, 25 (12), **1989**, 2665–2673. DOI: 10.1109/3.40655 (cited on page 13).